Supporting information for

Atomic Layer Deposition-Triggered Hierarchical Core/Shell Stable Bifunctional Electrocatalysts for Overall Water Splitting

T. Kavinkumar[a], Selvaraj Seenivasan[a], Hyeonjung Jung[b], Jeong Woo Han[b] and Do-Heyoung Kim[a]**

[a]School of Chemical Engineering, Chonnam National University, 77 Yongbong-ro, Gwangju 61186, Republic of Korea.

[b]Department of Chemical Engineering, Pohang University of Science and Technology (POSTECH), Pohang 37673, South Korea.

*Corresponding author's email: kdhh@chonnam.ac.kr; jwhan@postech.ac.kr

Tel. (office): +82-62-530-1894

Experimental section

The preparation of $NiCo_2O_4$, $NiCo_2O_4/MoO_2$, $NiCo_2O_4$@ALD-NiO and $NiCo_2O_4/MoO_2$@ALD-NiO heteronanostructures has been described in our previous report.[1]

Electrochemical measurements

A saturated calomel electrode (SCE), Pt foil, and as-fabricated samples on the nickel foam (NF) served as the reference, counter, and working electrodes, respectively in an electrochemical workstation (WonATech WBCS30000). Five milligrams of Pt/C (or RuO_2) and 10 μL of Nafion were dispersed in 1 mL of a water/alcohol mixture solution (3:1) using ultrasonication to prepare

an ink. Finally, 50 μL of the catalyst ink was coated on the NF followed by drying at 60 °C. Thereafter, LSV measurements were performed at 2 mV s^{-1} in a 1 M KOH solution for the OER and HER. EIS measurements were conducted on a Parstat 3000 workstation (0.01 Hz to 100 kHz at an amplitude of 10 mV). A gas chromatography system (074-594-P1E Micro GC Fusion, INFICON) was used to estimate the amounts of the gaseous products. All potentials were calibrated to the RHE using Eq 1. η was obtained using Eq 2, and the Tafel slope was obtained using Eq 3:

$$E_{RHE} = E_{SCE} + 0.059pH + 0.197 \quad (1)$$

$$\eta = E_{RHE} - 1.23 \quad (2)$$

$$\eta = b \log j + a \quad (3)$$

Computational details

All the DFT calculations were carried out using the Vienna Ab initio Simulation Package (VASP) [2, 3]. The Perdew–Burke–Ernzerhof exchange–correlation functional and the projector augmented wave pseudopotential were adopted with spin-polarization. During structural optimization, the convergence criterion of the total energy was set to 10^{-4} eV, and the atoms were relaxed until the force acting on each atom was less than 0.03 eV/Å [4, 5]. A plane-wave cutoff energy of 400 eV was used in all computations. Brillouin zone sampling was conducted with 6 × 6 × 6, 4 × 4 × 1, and 4 × 4 × 1 Monkhorst-Pack grids for the MoO_2 bulk, MoO_2 slab, and MoO_2@ALD-NiO slab model calculations, respectively [6]. The (-111) facet is typically studied in monoclinic MoO_2 systems, whereas the (100) facet is the most stable NiO surface [7-10]. Therefore, the most stable MoO_2 (-111) termination was investigated for the $NiCo_2O_4/MoO_2$

surface, and four NiO (100) layers were loaded onto it to represent the $NiCo_2O_4/MoO_2$@ALD-NiO surface (Figure S11). The lattice misfit between MoO_2 and NiO was calculated as follows:

$$f = \left| \frac{l_{MoO_2} - l_{NiO}}{l_{MoO_2}} \right|,$$

where l is the length of one side. The two bottom layers of the four MoO_2 layers were fixed in all slab models, and each slab model was separated from its neighbors by a sufficiently thick vacuum layer spacing. The Gibbs free energies of the alkaline OER and HER were calculated by correcting the DFT energy using the zero-point energy (*ZPE*) and entropy as follows:

$$\Delta G = \Delta E + \Delta ZPE - T\Delta S,$$

where E is the DFT-calculated total energy, *ZPE* is the zero-point energy, T is the environment temperature, and S is the entropy. The vibrational frequencies for the *ZPE* correction and entropy calculations were calculated by employing the density-functional perturbation theory.

The band center was calculated as follows:

$$M_d \text{ or } O_p = \frac{\int_{-\infty}^{E_f} E \cdot \rho(E) dE}{\int_{-\infty}^{E_f} \rho(E) dE},$$

where E_f is the Fermi-level energy, E is the energy relative to the Fermi level, and ρ represents the density of state in corresponding orbital.

Characterization

XRD patterns were collected from 10° to 80° using an X-ray diffractometer (PANalytical) employing Cu Kα radiation. FE-SEM and TEM were performed using the JEOL JSM-7500F and a Tecnai G2 F20, respectively. The oxidation states of the catalysts were determined using XPS (ESCALAB-MKII (VG Scientific Co.)).

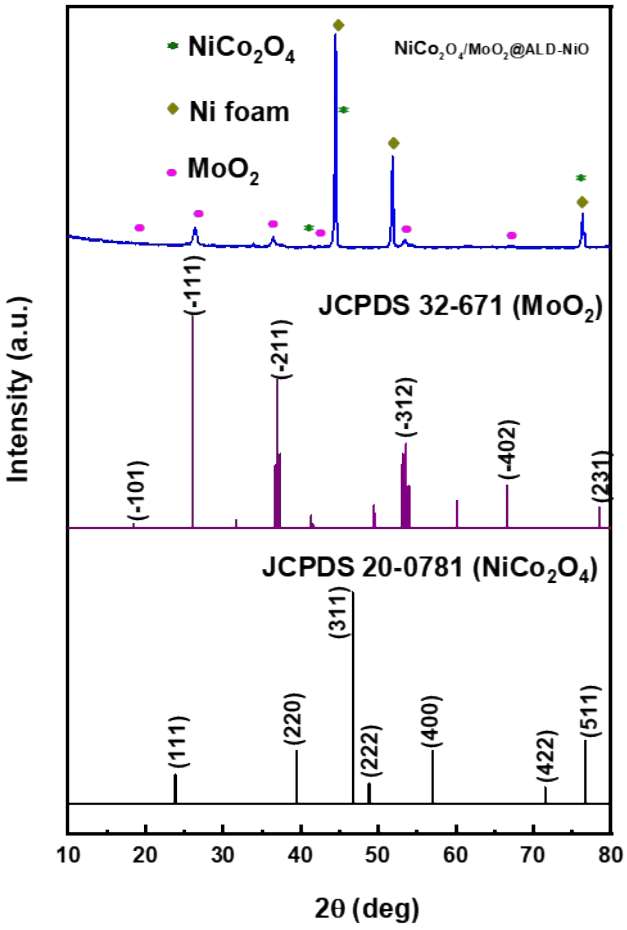

Figure S1. Powder XRD pattern of the $NiCo_2O_4/MoO_2$@ALD-NiO heteronanostructure. Reproduced with permission.[1]

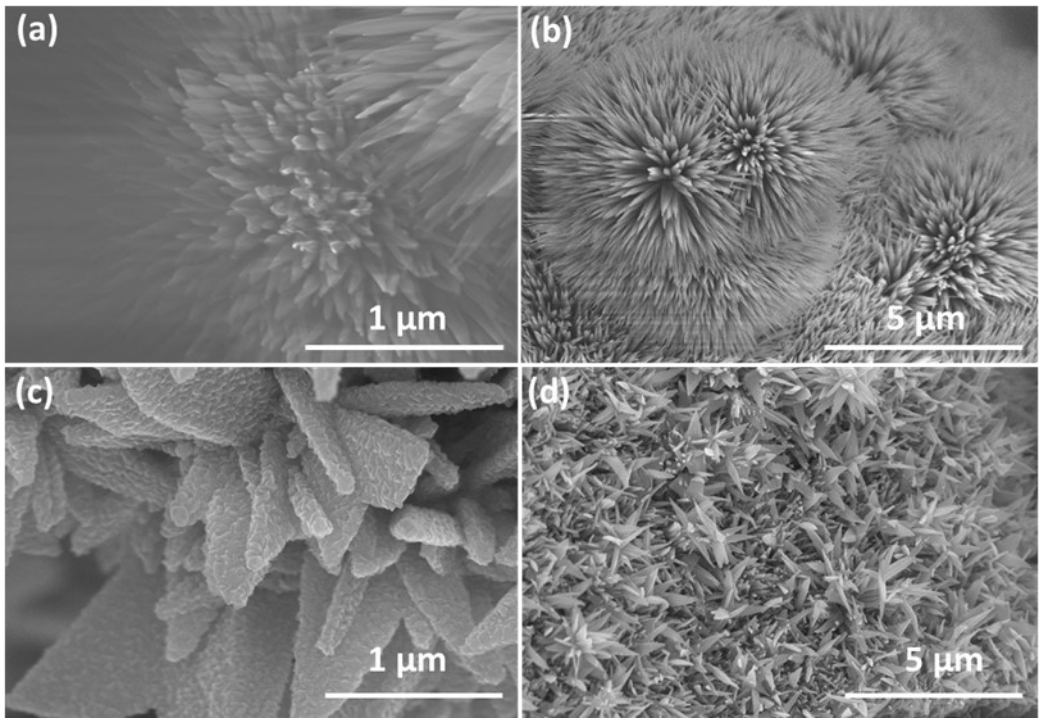

Figure S2. FE-SEM images of (a, b) pristine $NiCo_2O_4$, and the (c, d) $NiCo_2O_4/MoO_2$ core/shell structure at different magnifications. Reproduced with permission.[1]

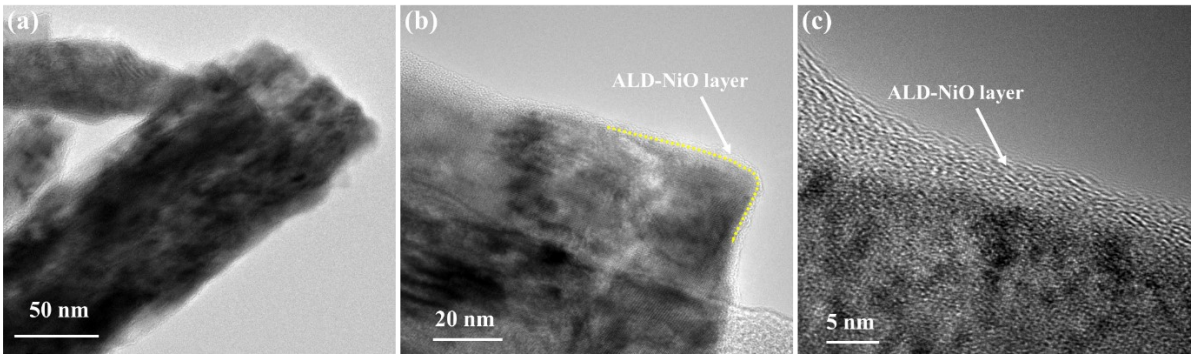

Figure S3. TEM images of $NiCo_2O_4$@ALD-NiO at different magnifications.

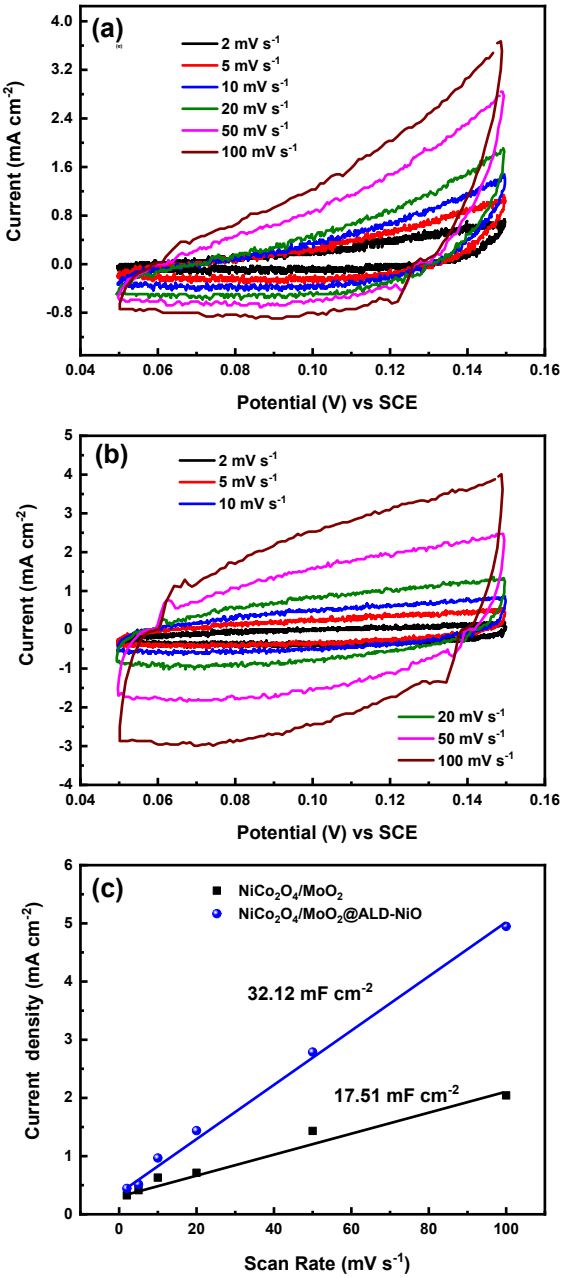

Figure S4. Cyclic voltammograms in the potential range 50–150 mV for (a) $NiCo_2O_4/MoO_2$ and (b) the $NiCo_2O_4/MoO_2$@ALD-NiO heteronanostructures at different sweep rates. (c) Current density vs. sweep rate of the as-prepared electrocatalysts for measuring C_{dl}.

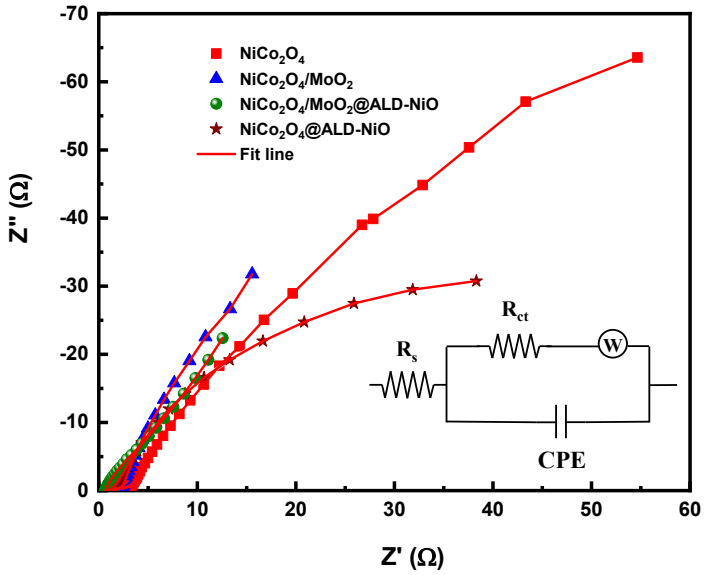

Figure S5. Nyquist plots corresponding to various catalysts in 1 M KOH.

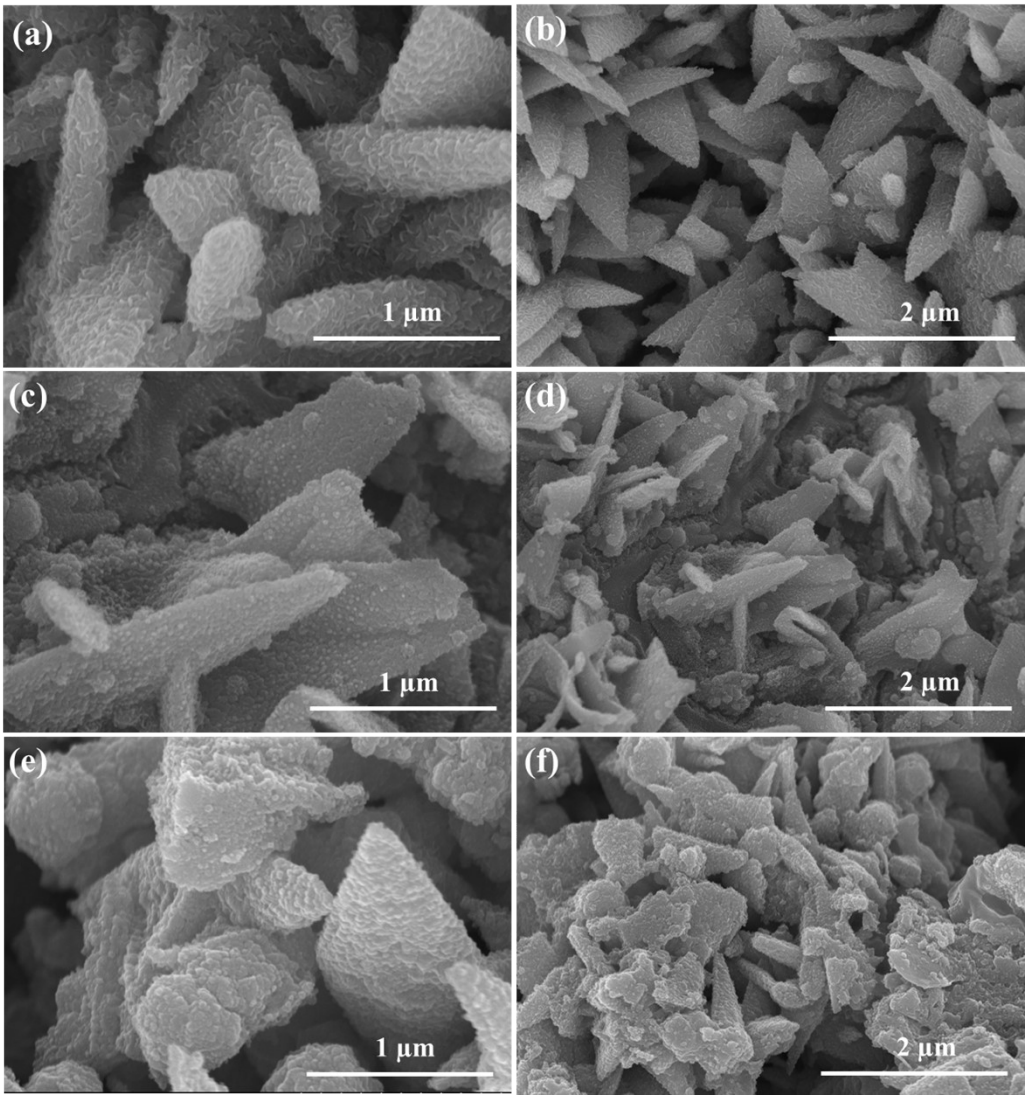

Figure S6. FE-SEM images of the $NiCo_2O_4/MoO_2$@ALD-NiO heteronanostructure (a, b) before, (c, d) after the100 h OER, and (e, f) after the 100 h HER.

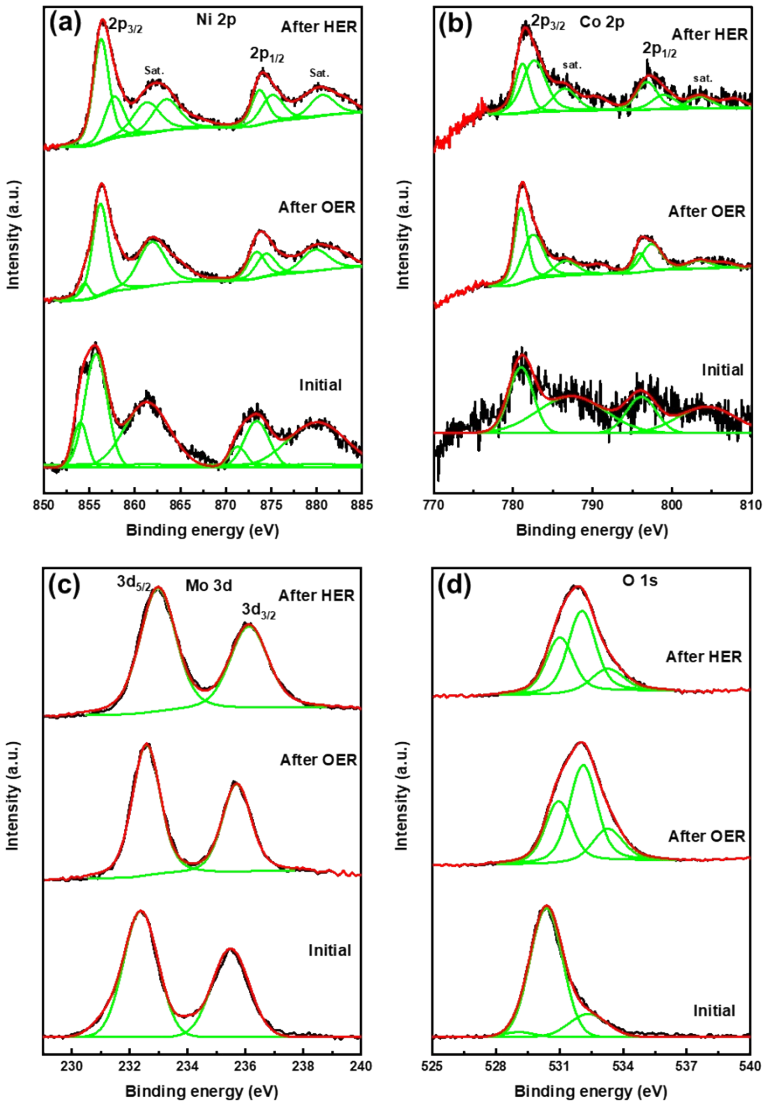

Figure S7. XPS spectra of the $NiCo_2O_4/MoO_2$@ALD-NiO heteronanostructure before and after 100 h of the OER/HER.

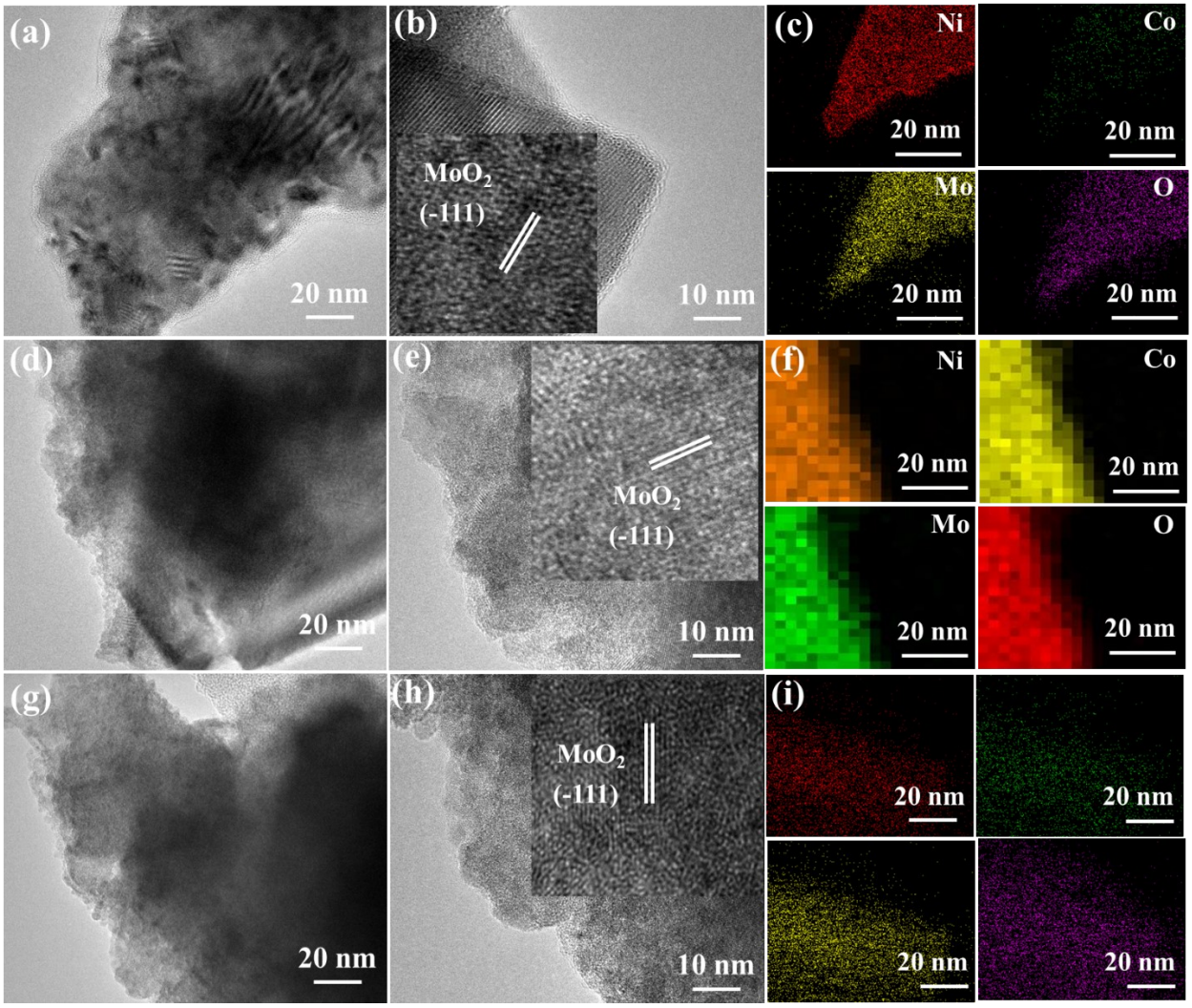

Figure S8. TEM, HR-TEM, and elemental mapping results for the $NiCo_2O_4/MoO_2$@ALD-NiO heteronanostructure: (a–c) before, (d–f) after the OER, and (g–i) after the HER.

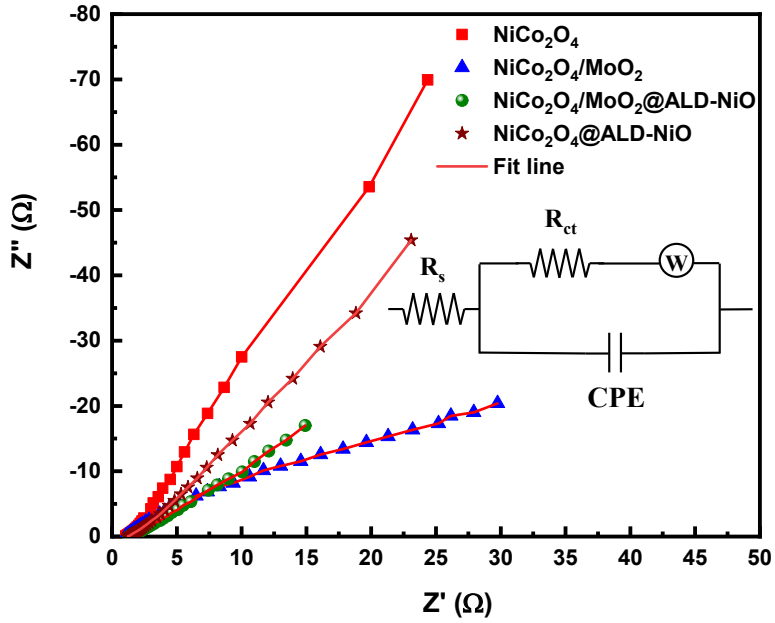

Figure S9. Nyquist plots corresponding to various catalysts in 1 M KOH.

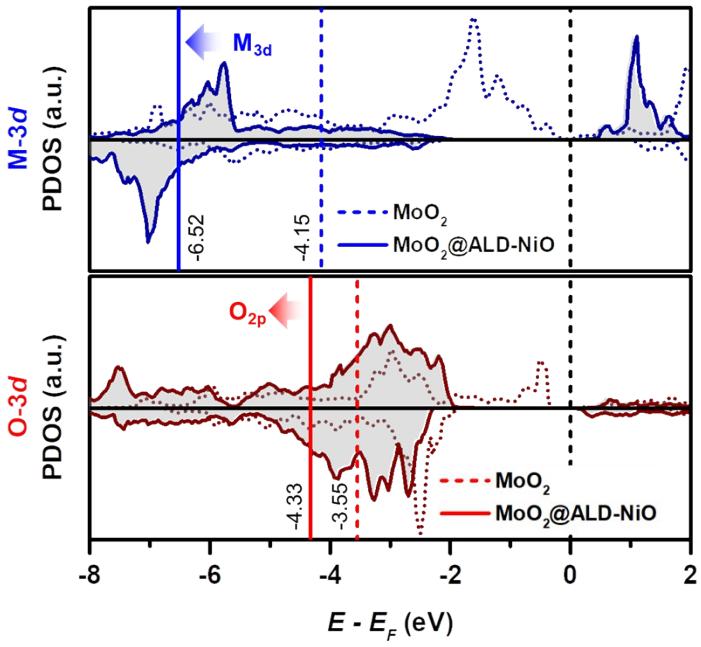

Figure S10. Partial density of states and band centers of the (a) active-metal 3d orbital and (b) active-oxygen 2p orbital. The Fermi level is set to zero.

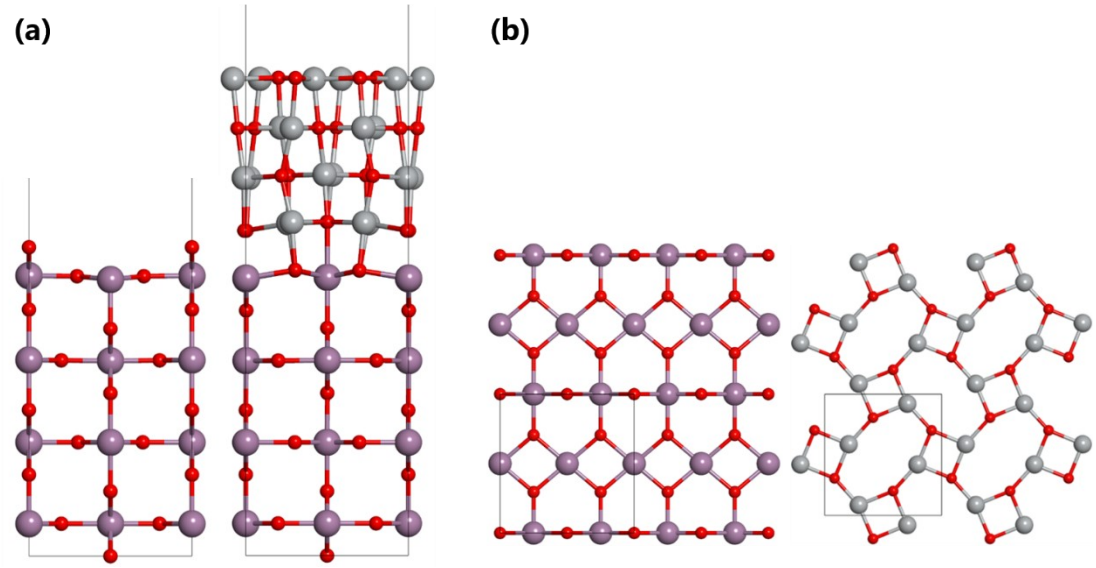

Figure S11. (a) Side and (b) top views of MoO_2 and MoO_2@ALD-NiO slab models, respectively. The solid black line represents one unit cell area.

Table S1. Comparison of the OER performance of the $NiCo_2O_4/MoO_2$@ALD-NiO heteronanostructure with that of previously reported electrocatalysts.

Catalyst	**Electrolyte**	**Overpotential at 100 mA cm^{-2} (mV)**	**Tafel slope (mV dec^{-1})**	**Ref.**
$NiCo_2O_4$@$CoMoO_4$	1 M KOH	~490	-	[11]
VCNB/NF	1 M KOH	370	-	[12]
$NiCo_2S_2$ NW	1 M KOH	370	40	[13]
Ni_2P@NF-6	1 M KOH	590	297	[14]
Ni@Co-Ni-P	1 M KOH	380	65	[15]
Ultrathin Co_3O_4 nanosheets	1 M KOH	535	49.1	[16]
NiCoP/C	1 M KOH	430	96	[17]
$Co_3O_4/NiCo_2O_4$	1 M KOH	495	88	[18]
NiFe-LDH	1 M NaOH	450	-	[19]
Co_3O_4 NWs	1 M KOH	468	95.0	[20]
$NiCo_2O_4/MoO_2$@ALD-NiO heteronanostructure	1 M KOH	**372.3**	**57.0**	**Present work**

Table S2. Comparison of the HER performance of the $NiCo_2O_4/MoO_2$@ALD-NiO heteronanostructure with that of previously reported electrocatalysts.

Catalyst	Electrolyte	Overpotential at 10 mA cm^{-2} (mV)	Tafel slope (mV dec^{-1})	Ref.
$NiCo_2O_4$@$CoMoO_4$	1 M KOH	121	77.0	[11]
Ni-Co-P	1 M KOH	107	46.0	[21]
NiFe-LDH/$NiCo_2O_4$	1 M KOH	192	59.0	[22]
$Ni(OH)_2$@CuS	1 M KOH	95	42.0	[23]
H-Fe-CoMoS	1 M KOH	138	98.0	[24]
$NiCo_2O_4$@$Ni_{0.796}$CoLDH	1 M KOH	115	56.4	[25]
Ar-$NiCo_2O_4$/S	1 M KOH	137	121.4	[26]
FeOOH/$NiCo_2O_4$	1 M KOH	146	41.3	[27]
$NiCo_2O_4$/NiCoP	1 M KOH	198	91.0	[28]
$NiCo_2O_4$ LDH nanoflakes	1 M KOH	140	124.2	[29]
$NiCo_2O_4$@$NiMoO_4$	1 M KOH	300	94.0	[30]
$NiCo_2O_4/MoO_2$@ALD-NiO heteronanostructure	1 M KOH	**57.1**	**58.0**	**Present work**

Table S3. Comparison of the water splitting performance of the $NiCo_2O_4/MoO_2$@ALD-NiO heteronanostructure with that of previously reported electrocatalysts.

Catalyst	Electrolyte	Voltage (V)	Ref.
$NiFe/NiCo_2O_4$	1 M KOH	1.67 V @ 10 mA cm^{-2}	31
Co-Fe oxyphosphide	1 M KOH	1.69 V @ 10 mA cm^{-2}	32
NiFe HNSs	1 M KOH	1.67 V @ 10 mA cm^{-2}	33
$NiS\text{-}Ni_2P_2S_6$	1 M KOH	1.64 V @ 10 mA cm^{-2}	34
$Ar\text{-}NiCo_2O_4/S$	1 M KOH	1.63 V @ 10 mA cm^{-2}	26
$NiCo_2O_4/NiCoP$	1 M KOH	1.66 V @ 10 mA cm^{-2}	28
$NiCo_2O_4//Ni_{0.33}Co_{0.67}S_2$ NWs	1 M KOH	1.73 V @ 10 mA cm^{-2}	35
Ni/NiO	1 M KOH	1.71 V @ 10 mA cm^{-2}	36
$CoxPO_4/CoP$	1 M KOH	1.91 V @ 10 mA cm^{-2}	37
$Co_9S_8\text{-}CoSe_2$	1 M KOH	1.66 V @ 10 mA cm^{-2}	38
$MoP@Ni_3P/NF$	1 M KOH	1.67 V @ 10 mA cm^{-2}	39
$NiCo_2O_4/MoO_2$@ALD-NiO heteronanostructure	**1 M KOH**	**1.62 V @ 10 mA cm^{-2}**	**This work**

References

1. T. Kavinkumar, S. Seenivasan, H. H. Lee, H. Jung, J. W. Han and D.-H. Kim, *Nano Energy*, 2021, **81**, 105667.
2. G. Kresse and J. Hafner, *Phys. Rev. B*, 1993, **47**, 558-561.
3. G. Kresse and J. Furthmüller, *Phys. Rev. B*, 1996, **54**, 11169-11186.
4. J. P. Perdew, K. Burke and M. Ernzerhof, *Phys. Rev. Lett.*, 1996, **77**, 3865-3868.
5. P. E. Blöchl, *Phys. Rev. B*, 1994, **50**, 17953-17979.
6. H. J. Monkhorst and J. D. Pack, *Phys. Rev. B*, 1976, **13**, 5188-5192.
7. K. Chen, X.-M. Zhang, X.-F. Yang, M.-G. Jiao, Z. Zhou, M.-H. Zhang, D.-H. Wang and X.-H. Bu, *Appl. Catal. B.*, 2018, **238**, 263-273.
8. H. H. Zhao, Z. Li, X. P. Dai, M. L. Cui, F. Nie, X. Zhang, Z. T. Ren, Z. H. Yang, Y. H. Gan, X. L. Yin, Y. Wang and W. Y. Song, *J. Mater. Chem. A*, 2020, **8**, 6732-6739.
9. P. W. Tasker and D. M. Duffy, *Surface Science*, 1984, **137**, 91-102.
10. B. C. Wang, J. Nisar and R. Ahuja, *ACS Appl. Mater. Interfaces*, 2012, **4**, 5691-5697.
11. Y. Q. Gong, Z. Yang, Y. Lin, J. L. Wang, H. L. Pan and Z. F. Xu, *J. Mater. Chem. A*, 2018, **6**, 16950-16958.
12. H. Han, Y. R. Hong, J. Woo, S. Mhin, K. M. Kim, J. Kwon, H. Choi, Y. C. Chung and T. Song, *Adv. Energy Mater.*, 2019, **9**, 1803799.
13. A. Sivanantham, P. Ganesan and S. Shanmugam, *Adv. Funct. Mater.*, 2016, **26**, 4661-4672.
14. J. L. Zheng, W. Zhou, T. Liu, S. J. Liu, C. B. Wang and L. Guo, *Nanoscale*, 2017, **9**, 4409-4418.
15. W. Li, X. F. Gao, X. G. Wang, D. H. Xiong, P. P. Huang, W. G. Song, X. Q. Bao and L. F. Liu, *J. Power Sources*, 2016, **330**, 156-166.

16. Z. Cai, Y. M. Bi, E. Y. Hu, W. Liu, N. Dwarica, Y. Tian, X. L. Li, Y. Kuang, Y. P. Li, X. Q. Yang, H. L. Wang and X. M. Sun, *Adv. Energy Mater.*, 2018, **8,** 1701694.

17. P. He, X. Y. Yu and X. W. Lou, *Angew. Chem. Int. Edit.*, 2017, **56**, 3897-3900.

18. H. Hu, B. Y. Guan, B. Y. Xia and X. W. Lou, *J. Am. Chem. Soc.*, 2015, **137**, 5590-5595.

19. J. S. Luo, J. H. Im, M. T. Mayer, M. Schreier, M. K. Nazeeruddin, N. G. Park, S. D. Tilley, H. J. Fan and M. Gratzel, *Science*, 2014, **345**, 1593-1596.

20. C. M. Zhang, F. Q. Zheng, Z. W. Zhang, D. Xiang, C. F. Cheng, Z. H. Zhuang, P. Li, X. K. Li and W. Chen, *J. Mater. Chem. A*, 2019, **7**, 9059-9067.

21. E. L. Hu, Y. F. Feng, J. W. Nai, D. Zhao, Y. Hu and X. W. Lou, *Energ. Environ. Sci.*, 2018, **11**, 872-880.

22. Z. Q. Wang, S. Zeng, W. H. Liu, X. W. Wang, Q. W. Li, Z. G. Zhao and F. X. Geng, *ACS Appl. Mater. Interfaces*, 2017, **9**, 1488-1495.

23. S. Q. Liu, H. R. Wen, Ying-Guo, Y. W. Zhu, X. Z. Fu, R. Sun and C. P. Wong, *Nano Energy*, 2018, **44**, 7-14.

24. Y. N. Guo, X. Zhou, J. Tang, S. Tanaka, Y. V. Kaneti, J. Na, B. Jiang, Y. Yamauchi, Y. S. Bando and Y. Sugahara, *Nano Energy*, 2020, **75,** 104913.

25. M. Li, L. Tao, X. Xiao, X. Jiang, M. Wang and Y. Shen, *ACS Sustain. Chem. Eng.*, 2019, **7**, 4784-4791.

26. J. H. Lin, Y. T. Yan, T. X. Xu, C. Q. Qu, J. Li, J. Cao, J. C. Feng and J. L. Qi, *J. Colloid. Interf. Sci.*, 2020, **560**, 34-39.

27. X. Cao, Y. Sang, L. Wang, G. Ding, R. Yu and B. Geng, *Nanoscale*, 2020, **12**, 19404-19412.

28. W. Jin, J. P. Chen, H. B. Wu, N. Zang, Q. W. Li, W. Q. Cai and Z. X. Wu, *Catal. Sci. Technol.*, 2020, **10**, 5559-5565.

29. L. B. Ma, Y. Hu, R. P. Chen, G. Y. Zhu, T. Chen, H. L. Lv, Y. R. Wang, J. Liang, H. X. Liu, C. Z. Yan, H. F. Zhu, Z. X. Tie, Z. Jin and J. Liu, *Nano Energy*, 2016, **24**, 139-147.

30. D. Cui, R. D. Zhao, J. Q. Dai, J. Xiang and F. F. Wu, *Dalton T.*, 2020, **49**, 9668-9679.

31. C. L. Xiao, Y. B. Li, X. Y. Lu and C. Zhao, *Adv. Funct. Mater.*, 2016, **26**, 3515-3523.

32. P. Zhang, X. F. Lu, J. W. Nai, S. Q. Zang and X. W. Lou, *Adv. Sci.*, 2019, **6,** 1900576.

33. X. H. Sun, Q. Shao, Y. C. Pi, J. Guo and X. Q. Huang, *J. Mater. Chem. A*, 2017, **5**, 7769-7775.

34. X. Y. Zhang, S. Zhang, J. Li and E. K. Wang, *J. Mater. Chem. A*, 2017, **5**, 22131-22136.

35. Z. Peng, D. S. Jia, A. M. Al-Enizi, A. A. Elzatahry and G. F. Zheng, *Adv. Energy Mater.*, 2015, **5,** 1402031.

36. H. Sun, Z. Ma, Y. Qiu, H. Liu and G.-g. Gao, *Small*, 2018, **14**, 1800294.

37. Y. Yang, H. L. Fei, G. D. Ruan and J. M. Tour, *Adv. Mater.*, 2015, **27**, 3175-3180.

38. S. Chakrabartty, S. Karmakar and C. R. Raj, *ACS Appl. Nano Mater.*, 2020, **3**, 11326-11334.

39. F. M. Wang, J. W. Chen, X. P. Qi, H. Yang, H. H. Jiang, Y. Q. Deng and T. X. Liang, *Appl. Surf. Sci.*, 2019, **481**, 1403-1411.